PHYSICAL REVIEW B **72**, 035337 (2005)

Theoretical investigation of electron-phonon interaction in one-dimensional silicon quantum dot array interconnected with silicon oxide layers

Shigeyasu Uno*
Hitachi Cambridge Laboratory, Hitachi Europe Ltd., Cavendish Laboratory, Madingley Road, Cambridge, CB3 0HE, United Kingdom

Nobuya Mori
Department of Electronic Engineering, Osaka University, 2-1 Yamada-oka, Suita, Osaka 565-0871, Japan

Kazuo Nakazato†
Department of Electrical Engineering and Computer Science, Graduate School of Engineering, Nagoya University, Furo-cho, Chikusa-ku, Nagoya 464-8603, Japan

Nobuyoshi Koshida†
Division of Electronic and Information Engineering, Faculty of Technology, Tokyo University of Agriculture and Technology, Tokyo 184, Japan

Hiroshi Mizuta†
Department of Physical Electronics, Tokyo Institute of Technology, 2-12-1 O-okayama, Meguro-ku, Tokyo 152-8552, Japan
(Received 3 August 2004; revised manuscript received 14 January 2005; published 18 July 2005)

Electronic and phononic states and their interactions in one-dimensional arrays of Si quantum dots interconnected with thin oxide layers is theoretically investigated. Electronic states under low electric field condition are obtained in the Kronig-Penny potential. Approximate expression for phonon wave functions is developed and numerically calculated using the linear atomic chain model. Simulated dispersion relation shows acoustic phonon modes, phonon band gaps, and confined optical phonon modes. Electron-phonon scattering rate is written using a one-dimensional expression. Intraminiband scattering rates and energy relaxation rates are simulated both for absorption and emission processes. The scattering rate varies from $\sim 10^{12}$ to $\sim 10^{14}$, depending on the initial electron energy. The scattering rate for absorption/emission processes rapidly decreases at near the top/bottom of minibands due to limited number of phonon branches that can mediate the scattering processes. Negative energy relaxation rate is observed near the bottom of minibands, which is due to larger scattering rate for absorption process and smaller phonon energy mediating the scatterings for emission process. The scattering rate for absorption decreases rapidly with decreasing temperature. Once the temperature drops down to 100 K, the energy relaxation rate for emission process dominates the absorption process.

DOI: 10.1103/PhysRevB.72.035337 PACS number(s): 73.63.Nm, 72.10.Di, 73.21.Cd

I. INTRODUCTION

The recent development of electron-beam lithography has enabled fabrication of the silicon quantum wires (SiQW) with lateral dimensions of several nanometers. Electron transport in such a structure has been systematically explored, and researchers have revealed various phenomena at low temperature such as the variable range hopping conduction,[1] single-electron behavior,[2,3] quantized conductance,[4–6] and quantum interference.[7,8] The porous silicon (PS) is the alternative of obtaining SiQW structure. The PS is formed on silicon substrates by electrochemical etching (chemical anodization), leading to self-assembled tree-like network of SiQW.[9,10] It is remarkable that, despite indirect band structure of Si, the PS shows efficient visible luminescence, which has greatly stimulated theoretical and experimental studies.[11] More interestingly, there are reports of high-energy electron emission at room temperature.[12–14] Similar structure also exhibits the electron emission.[15] Energy distribution of emitted electrons have been studied in detail.[16] Recently, theoretical calculation of electron transport properties in SiQW was made by Sanders *et al.*.[17] The electronic states were obtained from an empirical tight-binding calculation, and scattering rates were calculated to perform Monte Carlo simulation of electron transport. However, most of PS light/electron emission devices undergo an oxidation process,[9] and the SiQWs in the PS are rather one-dimensional arrays of Si quantum dots interconnected with thin oxide layers (1DSiQDA).[9,12,13] Therefore, theoretical study of the 1DSiQDA, rather than simple SiQW structure, should be done. Such study also gives insights into electronic behaviors in similar Si/SiO_2 coupled structures investigated for quantum computation and memory applications.[18,19]

In this paper, we theoretically investigate the electronic/phononic states and their interactions in an ideal 1DSiQDA structure under low electric field condition. Temperature dependence of phonon scattering rate and energy relaxation rate are also investigated.

We present in Sec. II a theoretical framework to calculate the electron-phonon interactions in the 1DSiQDA. In Sec. III, we show numerical calculation results of electronic and phononic states, as well as electron phonon interactions. Sev-

 ©2005 The American Physical Society

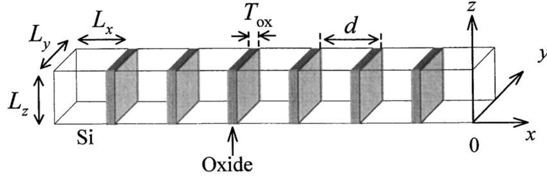

FIG. 1. Model of the idealized one-dimensional Si quantum dot array interconnected with thin oxide layers (1DSiQDA).

eral issues are discussed in Sec. IV, and Sec. V is devoted to concluding remarks.

II. THEORY AND SIMULATION

A. Model

Figure 1 shows schematic illustration of our idealized model of the 1DSiQDA. The x, y, and z axes are set as shown in the figure, and the Si dots are modeled as cubes of L_x, L_y, and L_z each side. These Si dots are interconnected by oxide layers of thickness T_{ox}. The period of this structure in the x direction, d, is therefore given by $d = L_x + T_{\mathrm{ox}}$. This array of Si dots infinitely extends in the x direction, and it is assumed to be surrounded by vacuum.

Major phonon scattering mechanism in the 1DSiQDA is the deformation potential scattering. Although the oxide layers are polar material, the polar-optical phonon scattering from those layers would be negligible as far as T_{ox} is small compared to L_x. The deformation potential scattering in similar structure was investigated in detail by Noguchi *et al.*[20] and Stocker *et al.*[21] They assumed bulk acoustic phonons in one-dimensional coupled quantum-box structures of $\mathrm{GaAs/Al}_x\mathrm{Ga}_{1-x}\mathrm{As}$ heterostructure. The assumption of bulk phonon is valid in their case, because there is almost no mechanical mismatch between GaAs and $\mathrm{Al}_x\mathrm{Ga}_{1-x}\mathrm{As}$ [85.3 $-1.8x$ GPa (see Ref. 22)]. However, it is not the case in the 1DSiQDA, because there is considerable difference in the mechanical properties of the Si and the oxide layer; the Young's moduli for Si and SiO_2 film are 180 and 70 GPa, respectively.[23,24] Therefore, the periodic mechanical mismatch of the structure should be properly considered in our calculation, which alters some of the techniques employed in the reports from Noguchi and Stocker.

B. Electronic states

In the SiQW, there are three energy minima in the $\mathbf{k}$ space; that is, two X valleys and one Γ-like valley on the k_x axis.[17] However, in the 1DSiQDA, the two X valleys are folded into smaller first Brillouin zone ranging $-\pi/d < k_x < \pi/d$. As a result, these folded X valleys are mixed with the Γ-like valley, forming a new single valley near $k_x = 0$. In this paper, we employ the effective mass approximation in this single valley.

As we assume low electric field applied across the 1DSiQDA, the Schrödinger equation is solved in the Kronig-Penny potential. Strictly speaking, the equation cannot be separated in terms of three coordinates, because the effective mass for electron is different in Si and oxide layers. However, to simplify the calculation, we assume that the simple approach of variable separation in the literatures[20,21] can be used in the 1DSiQDA. This is acceptable because the electron effective masses in Si and SiO_2 are relatively close [0.33 and 0.42, respectively (see Ref. 25)]. The solution to the Schrödinger equation is then written as

$$\begin{cases} \langle x|k_x b_e\rangle = \dfrac{1}{\sqrt{L}} u_{k_x,b_e}(x) e^{i\,k_x x}, \\ \langle y|n_y\rangle = \sqrt{\dfrac{2}{L_y}} \sin\left[\dfrac{n_y \pi}{L_y} y\right], \\ \langle z|n_z\rangle = \sqrt{\dfrac{2}{L_z}} \sin\left[\dfrac{n_z \pi}{L_z} z\right], \end{cases} \tag{1}$$

where b_e is the band index, L is length of the 1DSiQDA in the x direction, n_y and n_z take natural numbers, and $u_{k_x,b_e}(x)$ is the Bloch function.

The total energy E_{total} is given by

$$E_{\mathrm{total}} = E_x(k_x, b_e) + \frac{\pi^2 \hbar^2}{2m^*}\left(\frac{n_y^2}{L_y^2} + \frac{n_z^2}{L_z^2}\right), \tag{2}$$

where m^* is the electron effective mass. The x energy component $E_x(k_x, b_e)$ and the Bloch function $u_{k_x,b_e}(x)$ are easily obtained by solving the Schrödinger equation in a given periodic potential profile. Although we have ignored the difference in the effective masses in Si and oxide in the above derivation, we took into account of the difference in the calculation of the Bloch states $u_{k_x,b_e}(x)$ to minimize the error due to the assumption.

C. Phononic states

Acording to Morse,[26] the phonon normal modes in a quantum wire having square cross sections can be given by

$$\mathbf{v}_{\mathbf{Q}}(\mathbf{R}) e^{i q_x x}, \tag{3}$$

where $e^{i q_x x}$ is a plane wave propagating in the x direction, q_x is the phonon wave vector, and $\mathbf{v}_{\mathbf{Q}}$ is a vector as a function of $\mathbf{R}$ and $\mathbf{Q}$ defined as

$$\mathbf{R} = \begin{pmatrix} y \\ z \end{pmatrix}, \quad \mathbf{Q} = \begin{pmatrix} q_y \\ q_z \end{pmatrix}. \tag{4}$$

The vector $\mathbf{v}_{\mathbf{Q}}(\mathbf{R})$ includes the trigonometric functions, and is often approximated as plane waves having antinodes at the side edge of the structure.[20,27,28] This is also true in the 1DSiQDA. However, the x component is no longer a plane wave because of the large mechanical mismatch between Si dots and oxide layers, as discussed in the previous subsection. Therefore the phonon wave functions in the 1DSiQDA are written as

$$\begin{cases} \mathbf{S}(\mathbf{r}) = \displaystyle\sum_{\mathbf{q}} C_{\mathbf{q}} (a_{\mathbf{q}} + a_{-\mathbf{q}}^{+}) e^{i\,\mathbf{Q}\cdot\mathbf{R}} S_{q_x}(x) \mathbf{s}_{\mathbf{q}}, \\ C_{\mathbf{q}} \equiv \sqrt{\dfrac{\hbar}{2\omega_{\mathbf{q}}} \frac{1}{N_y N_z}}, \end{cases} \tag{5}$$

where $\mathbf{q}$ is the phonon wave vector, $a_{-\mathbf{q}}^{+}$ and $a_{\mathbf{q}}$ are the creation and annihilation operators, $S_{q_x}(x)$ is a one-dimensional

phonon wave, $\mathbf{s_q}$ is the unit vector in the direction of atomic vibrations, $\omega_\mathbf{q}$ is the frequancy of the phonon vibration, and N_yN_z is the total number of atoms in a cross section.

The function $S_{q_x}(x)$ is numerically obtained using the linear atomic chain model shown in Fig. 2. In this model, the 1DSiQDA consists of Si region containing only Si atoms and the oxide region containing Si and O atoms alternating with each other. The lattice potential energy is expanded as a power series of the displacement of the atoms from their minimum energy positions, but only to the second order. This leads to atomic force proportional to the displacement. The proportional coefficient acts as "spring constant" of a bond. As we are interested in the first-order effects, we consider interaction between the nearest atoms only. In addition electrical force caused by dipole momentum of Si–O bond was neglected, that is, the oxide layers are treated as nonpolar material. Therefore, the optical interface mode does not appear in our simulation, as in GaAs/AlGaAs systems. The distance between the neighboring atoms (a) was determined from the mass density of atoms in Si, and we used the same distance for Si–O bonds. The number of atoms included in a Si or SiO_2 region were obtained by dividing the size by a. The number of atoms in a period (N_{unit}) is then given by d/a. The mass of Si and O atoms were set based on their atomic weights. The spring constant between each Si–Si bond (K_{Si-Si}) was determined so that the phonon maximum energy obtained by the calculation for the SiQW is identical to the maximum energy of longitudinal phonons in bulk Si (100) direction. The spring constant between each Si–O bond, K_{Si-O}, was determined from the ratio of Young's modulus for bulk Si and SiO_2 film.

The phonon normal modes and energy dispersion relation are obtained by solving equations of motion for these atoms under periodic boundary condition.[29] The equations of motion reduce to an eigenequation for phonon normal modes. The eigenvectors give phonon wave functions $S_{q_x}(x)$, and the eigenenergies as a function of phonon wave vector q_x give the dispersion relation. Because of the periodic nature of the structure, the phonon dispersion relation is folded into smaller first Brillouin zone with the edge value of π/d. As a result, there are N_{unit} phonon branches in the first Brillouin zone.

D. Electron-phonon interaction

1. Acoustic and optical deformation potential scattering

The probability of the transition from an initial electronic/phononic state $|\mathbf{k}c\rangle$ to a final state $|\mathbf{k}'c'\rangle$ is calculated using Fermi's golden rule, and the perturbation Hamiltonian for the acoustic deformation potential (ADP) scattering can be written as[30]

$$H_{ADP}(\mathbf{r}) = D_{aco}\nabla\cdot\mathbf{S}(\mathbf{r}) \tag{6}$$

Using the phonon wave function Eq. (5), the matrix element reads

$$\langle\mathbf{k}'\,c'|H_{ADP}(\mathbf{r})|\mathbf{k}\,c\rangle = D_{aco}\begin{pmatrix} C_\mathbf{q}\sqrt{n_\mathbf{q}} \\ C_{-\mathbf{q}}\sqrt{n_{-\mathbf{q}}+1}\end{pmatrix}\langle n_y'n_z'|e^{\pm i\,\mathbf{Q}\,\mathbf{R}}|n_yn_z\rangle \times\left\{\pm i(q_ys_{\pm q,y}+q_zs_{\pm q,z})\langle k_x'b_e'|S_{\pm q_x}(x)|k_xb_e\rangle + s_{\pm q,x}\langle k_x'b_e'|\frac{\partial S_{\pm q_x}(x)}{\partial x}|k_xb_e\rangle\right\}. \tag{7}$$

The integral in the y and z directions is the Fourier transform of a function localized within $0<y<L_y$ and $0<z<L_z$. Therefore the integral is nonzero only when the y and z components of the phonon wave vectors satisfy $q_y\sim 1/L_y$ and $q_z\sim 1/L_z$. For $L_y=L_z=4$ nm, which is typical Si dot size in the literatures,[13,14,31] a phonon vector satisfying the above criteria has energy of $\sim$1 meV in the y and z directions. As the x component of the phonon energy can range up to about 60 meV,[32] majority of phonons contributing to the electron-phonon scattering have wave vector parallel to the x axis. Therefore, we can approximate the matrix element as

$$|\langle\mathbf{k}'\,c'|H_{ADP}|\mathbf{k}\,c\rangle|^2 \propto \left|\langle k_x'b_e'|D_{aco}\frac{\partial S_{\pm q_x}(x)}{\partial x}|k_xb_e\rangle\right|^2 \tag{8}$$

and the transition probability is written as

$$\begin{cases} T(\mathbf{k}\to\mathbf{k}') = \dfrac{2\pi}{\hbar}\dfrac{\hbar}{2\omega_{\pm q_x}}\dfrac{1}{N_yN_z}\begin{Bmatrix} n_{q_x} \\ n_{-q_x}+1\end{Bmatrix}\left(1+\dfrac{1}{2}\delta_{n_yn_y'}\right)\left(1+\dfrac{1}{2}\delta_{n_zn_z'}\right)|\langle k_x'b_e'|H_{\text{el-ph}}(x)|k_xb_e\rangle|^2\delta[E(\mathbf{k}')-E(\mathbf{k})\mp\hbar\omega_{\pm q_x}], \\ H_{\text{el-ph}}(x)\equiv D_{aco}\dfrac{\partial S_{\pm q_x}(x)}{\partial x}, \end{cases} \tag{9}$$

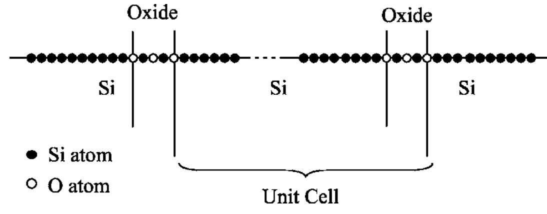

FIG. 2. Linear atomic chain model used for phonon calculation.

where the integral in the y and z directions was performed using the formula in the literature.[33]

Same result is obtained for the optical deformation potential (ODP) scattering, and the one-dimensional scattering potential is written as

$$H_{\text{el-ph}}(x) = D_{\text{opt}} S_{\pm q_x}(x). \tag{10}$$

Thus, in the 1DSiQDA, the transition probability can be reduced to a one-dimensional expression.

2. General form of deformation potential scattering

In the 1DSiQDA, phonon scatterings occur in a single-electron energy minimum located in $-\pi/d < k_x < \pi/d$. These scattering processes are mediated by N_{unit} phonon branches folded in $-\pi/d < q_x < \pi/d$. Therefore, phonons at any energy could contribute to the phonon scattering, and we need to extend the expression Eq. (9) to be applicable to scatterings mediated by arbitrary energy phonons. Such an issue is unique to the 1DSiQDA, and cannot be seen in the SiQW or the one-dimensional coupled quantum-box structures of $GaAs/Al_xGa_{1-x}As$.

In principle, the deformation potential is defined as the change in the electron conduction band minimum caused by the local change in lattice spacing.[34] This can be formally expressed as

$$H_{\text{el-ph}}(x) = D\frac{\delta a}{a}, \tag{11}$$

where a is the lattice spacing at position x. Using the one-dimensional phonon wave function, this can be written as

$$H_{\text{el-ph}}(x) = D\frac{S_{q_x}(x+a) - S_{q_x}(x)}{a}. \tag{12}$$

This expression is valid for phonons at any energy. Note that this expression should approach to the perturbation Hamiltonian for ADP scattering as the phonon wave length becomes much larger than a, and that for the ODP as the wavelength becomes comparable to a. The coupling constant D in the Eq. (12) must then satisfy

$$\begin{cases} D\dfrac{\partial S_{q_x}(x)}{\partial x} = D_{\text{aco}}\dfrac{\partial S_{q_x}(x)}{\partial x} & \text{(at acoustic limit)}, \\ D\dfrac{2}{a}S_{q_x}(x) = D_{\text{opt}} S_{q_x}(x) & \text{(at optical limit)}. \end{cases} \tag{13}$$

In order that the coupling constant D satisfy these conditions, it should vary depending on the phonon modes. In this work, we assume

$$D(\hbar\omega) = D_{\text{aco}} + \frac{\hbar\omega}{\hbar\omega_{\max}}\left(\frac{a}{2}D_{\text{opt}} - D_{\text{aco}}\right). \tag{14}$$

Such a phonon-dependent coupling constant has been reported for bulk material by Zoilner *et al.*[35]

The scattering rate mediated by one phonon branch b_p is given by the sum of all possible transition as

$$W_{b_p}(k_x,b_e) = \frac{d}{2\pi}\sum_j \frac{\tilde{T}(k_x b_e \to k_x' b_e')}{|F'(k_x' = k_j')|}, \tag{15}$$

where

$$\begin{cases} \tilde{T}(k_x b_e \to k_x' b_e') \equiv \dfrac{T(k_x b_e \to k_x' b_e')}{\delta[E(k_x',b_e') - E(k_x,b_e) \mp \hbar\omega_{\pm q_x}]}, \\ F(k_x',b_e') \equiv E(k_x',b_e') - E(k_x,b_e) \mp \hbar\omega_{\pm q_x} \end{cases} \tag{16}$$

and $k_j'(j=1,2,\ldots)$ is the jth root of $F(k_x',b_e')=0$.

The scattering rate as a function of initial electronic state is then obtained by summing for all phonon branches as

$$W(k_x,b_e) = \sum_{b_p=1}^{N_{\text{unit}}} W_{b_p}(k_x,b_e). \tag{17}$$

This is calculated for absorption and emission processes.

The energy relaxation rate is calculated using[36]

$$R_{\text{relax}} = \frac{d}{2\pi}\sum_j \frac{\tilde{T}(k_x b_e \to k_x' b_e')}{|F'(k_x' = k_j')|}\left(\mp\frac{\hbar\omega_{\pm q_x}}{E(k_x,b_e)}\right), \tag{18}$$

where upper and lower sings denote absorption and emission processes, respectively.

Finally, the parameters used in our simulations are listed in Table I.

III. RESULTS

A. Electronic states

Figure 3(a) shows electron eigenenergies in the 1DSiQDA as a function of electron wave vector in the x direction. The broken line shows the barrier height of the oxide layers. The horizontal axis is normalized to the edge value of the first Brillouin zone, π/d. The energy levels of the electrons are grouped in so called minibands, each of which corresponds to a quantized level for motion in the x direction. The energy gaps between minibands are called minibandgaps. For comparison, the result calculated for one-dimensional coupled quantum-box structures of GaAs/AlAs (1DGaAsQDA) is

TABLE I. Parameters used in our simulation.

Parameter	Symbol [unit]	Value
Si dot size	L_x, L_y, L_z[nm]	4.0 (Ref. 31)
Oxide thickness	T_{ox}[nm]	1.0 (Ref. 37)
Period	d[nm]	5.0
Electron effective mass in Si	m^*_{Si}	0.33 (Ref. 25)
Electron effective mass in oxide	m^*_{ox}	0.42 (Ref. 25)
Oxide barrier height	V[eV]	1.0 (Ref. 37)
Atom spacing	a[nm]	0.25 (see text)
Number of atoms in a unit cell	N_{unit}	20 (see text)
Atomic mass of Si	M_{Si}[kg]	46.622×10^{-27} (see text)
Atomic mass of O	M_O[kg]	26.559×10^{-27} (see text)
Spring constant Si–Si	K_{Si-Si}[N/m]	103.4 (see text)
Spring constant Si–O	K_{Si-O}[N/m]	41.36 (see text)
Acoustic deformation potential in Si	D_{aco}[eV]	9.0 (Ref. 30)
Acoustic deformation potential in oxide	D_{aco}[eV]	3.5 (Ref. 38)
Optical deformation potential in Si	D_{opt}[eV/cm]	11×10^8 (Ref. 30)
Optical deformation potential in oxide	D_{opt}[eV/cm]	20×10^8 (Ref. 39)

shown in Fig. 3(b). The barrier height is 0.75 eV, and the effective masses in GaAs and AlAs are set 0.067 and 0.150, respectively.[41]

Note that the minibands are more closely spaced in the 1DSiQDA than in the 1DGaAsQDA. This is due to the large electron effective masses in Si and the oxide layers compared to those in GaAs and AlAs. As a result, the minibands in the 1DSiQDA are less dispersive than those in the 1DGaAsQDA, indicating larger miniband effective mass and hence less electron mobility in the 1DSiQDA.

B. Phononic states

Figure 4(a) shows phonon dispersion relation in the 1DSiQDA. The horizontal axis shows the phonon wave vector q_x and is normalized to π/d. The phonon energy gaps (also known as phonon stop bands[40]) are observed, and the longitudinal acoustic sound velocity decreases about 16% compared to the result obtained from Si. In the energy range of $0.025\ \text{eV} < \hbar\omega < 0.035\ \text{eV}$, the phonon branches are nearly flat, and those in $0.045\ \text{eV} < \hbar\omega$ are completely dispersionless. These characteristics are qualitatively explained by comparing with dispersion relations calculated for Si and oxide quantum wires. Figure 4(b) shows phonon dispersion in SiQW, which was calculated using an atomic chain consisting of Si atoms only. In the calculation, all the O atoms in Fig. 2 were replaced by Si atoms, and the spring constant for Si, $K_{\text{Si-Si}}$, was used all over the structure. Figure 4(c) shows the dispersion relation for oxide quantum wire, which was calculated using an atomic chain consisting of Si and O atoms alternating with each other. In this calculation, $K_{\text{Si-O}}$ was used all over the structure, and the electrical force caused by dipole momentum of Si–O bond was neglected. In these two limiting cases, the edge value of the first Brillouin zone is

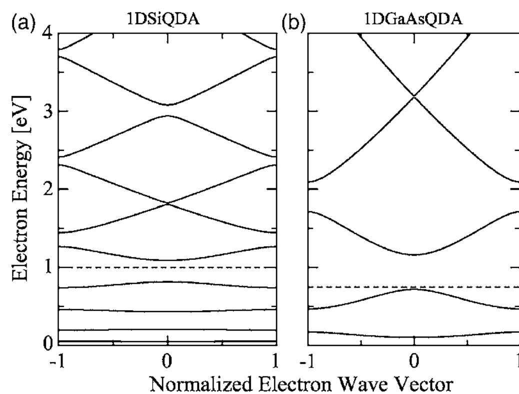

FIG. 3. One-dimensional electron energy dispersion in (a) 1DSiQDA and (b) one-dimensional coupled quantum-box structures of GaAs/AlAs (1DGaAsQDA). The horizontal axis is normalized to the edge value of the first Brillouin zone, π/d. Broken line shows the barrier height. Parameters used in the calculation for the 1DSiQDA is shown in Table I. For the 1DGaAsQDA, the barrier height is 0.75 eV, and the effective masses in GaAs and AlAs are set 0.067 and 0.150, respectively.

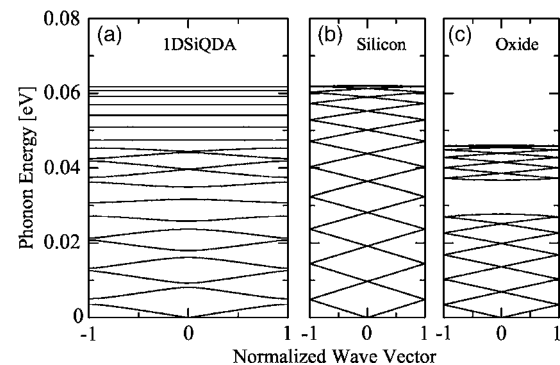

FIG. 4. One-dimensional phonon energy dispersions for (a) 1DSiQDA (b) Si quantum wire, and (c) oxide quantum wire. The horizontal axis is normalized to the edge value of the first Brillouin zone, π/d.

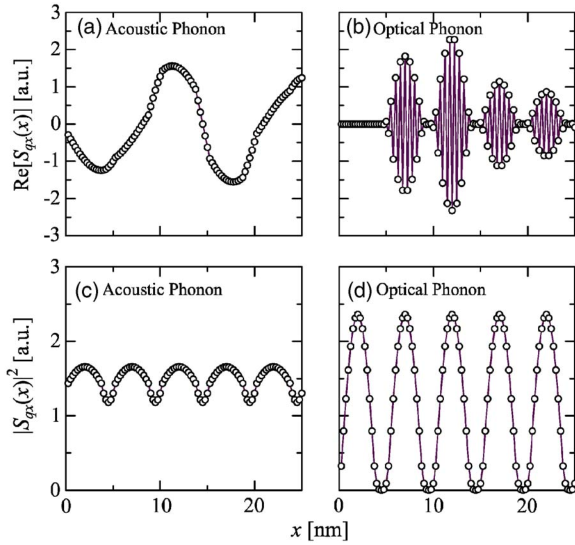

FIG. 5. (Color online) One-dimensional phonon wave functions in the 1DSiQDA, $S_{q_x}(x)$. (a) Real part of $S_{q_x}(x)$ calculated for an acoustic phonon having phonon energy of 0.003 eV. (b) Same plot for an optical phonon. (c) Squared amplitude of the acoustic phonon wave shown in (a). (d) Squared amplitude of the optical phonon wave shown in (b).

larger than π/d. However, the dispersion relations are folded into $-\pi/d < q_x < \pi/d$ and the wave vector is normalized to π/d for visualization. In Fig. 4(b), the phonon dispersion is continuous in energy, while that in Fig. 4(c) clearly shows optical branch ($0.035\text{ eV} < \hbar\omega < 0.045\text{ eV}$) and acoustic branch ($\hbar\omega < 0.025\text{ eV}$). In the 1DSiQDA, phonon vibration can exist both in the Si dots and the oxide layers only when phonon energy is within $\hbar\omega < 0.025\text{ eV}$ or $0.035\text{ eV} < \hbar\omega < 0.045\text{ eV}$. Such phonon normal modes should be characterized by a parameter of translational symmetry, that is, q_x, and therefore the phonon branches have certain dispersion. The phonon dispersion is then a "mixture" of those in Figs. 4(b) and 4(c). The phonon energy gaps appeared because of the mismatch of the spring constants in the Si dot region and the oxide layers.[42] On the other hand, when phonon energy lies in $0.025\text{ eV} < \hbar\omega < 0.035\text{ eV}$ or $0.045\text{ eV} < \hbar\omega$, such phonon vibration cannot exist in the oxide layers, and therefore it is localized only in the Si dot regions. Such localized phonons are not affected by q_x, and hence the phonon branches are dispersionless.

Figure 5(a) shows the real part of an acoustic phonon wave function, Re[$S_{q_x}(x)$], having phonon energy of 0.003 eV. The regions $5.0n - 1.0 < x < 5.0n$, ($n = 1,2,\ldots$) correspond to oxide layers. Each open circle represents an atom, and the interpolating solid line is merely for visualization. The wave form apparently differs from a plane wave expected in the SiQW, and is distorted at the oxide layers. In the oxide layers, difference of the displacement between neighboring atoms is larger than that in the Si dot region. This is due to the fact that the atoms tend to be separated apart because of smaller spring constant in the oxides. Figure 5(c) shows squared amplitude of the acoustic phonon wave, $|S_{q_x}(x)|^2$. The phonon vibration occurs all over the 1DSiQDA as mentioned above. Note that the amplitude is larger in the Si dot regions than in the oxide layers. This indicates that the atoms in the Si dots are far more displaced from their equilibrium position than those in the oxide layers. This leads to large phonon-generated strain in the oxide layers.[16] Figures 5(b) and 5(d) show Re[$S_{q_x}(x)$] and $|S_{q_x}(x)|^2$ for an optical phonon wave at the highest phonon branch, respectively. As mentioned above, the optical phonon vibrations are confined in the Si dot regions.

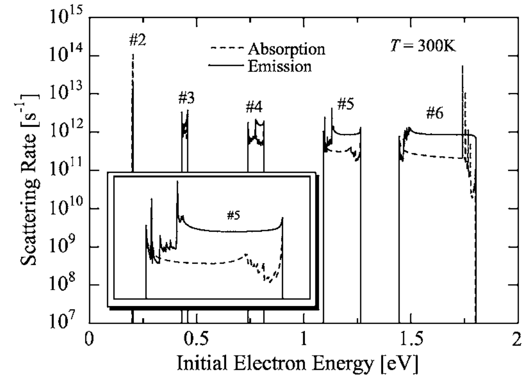

FIG. 6. Scattering rates as a function of initial electron energy calculated for absorption (broken lines) and emission (solid lines) processes. Each group of curves was obtained from the second to sixth electron minibands. The calculation was performed at $T = 300$ K. The inset is the blow-up of the results calculated for the fifth miniband.

C. Intraminiband scattering

Figure 6 shows the scattering rates W as a function of initial electron energy calculated using Eq. (17). The broken lines and the solid lines show results of phonon absorption and emission processes, respectively. The calculation was performed at $T = 300$ K. Each group of curves was obtained from the second to sixth lowest electron minibands. We could not calculate intra-miniband scattering for the 1st lowest miniband, because the dispersion of the miniband was much smaller than that of the lowest phonon branch. The inset is a blow-up of the curves calculated for the fifth miniband. The sharp spikes occur when the final electron state approaches to the miniband minimum or maximum, where the denominator in Eq. (15) approaches to zero. The scattering rate for the second miniband is of the order of 10^{14}, and it decreases by two orders of magnitude as the miniband index increases. This decrease of the scattering rate attributes to the decrease of the density of states caused by the increase of the miniband dispersion seen in Fig. 3(a). The scattering rates are slightly higher than that calculated for bulk Si.[30] The scattering rate for emission is 2 to 3 times larger than that for absorption. This is caused by the term $n_{\mathbf{q}}$ and $n_{-\mathbf{q}} + 1$ in Eq. (9). This difference vanishes at high temperatures. Note that the scattering rate for absorption/emission processes rapidly decreases at near the top/bottom of minibands. In order to understand this, we plotted in Fig. 7 the scattering rate (absorption) for electrons in the fifth miniband mediated by (a) the lowest to the fifth phonon branch, (b) sixth to tenth, (c) eleventh to fifteenth, and (d) sixteenth to twentieth.

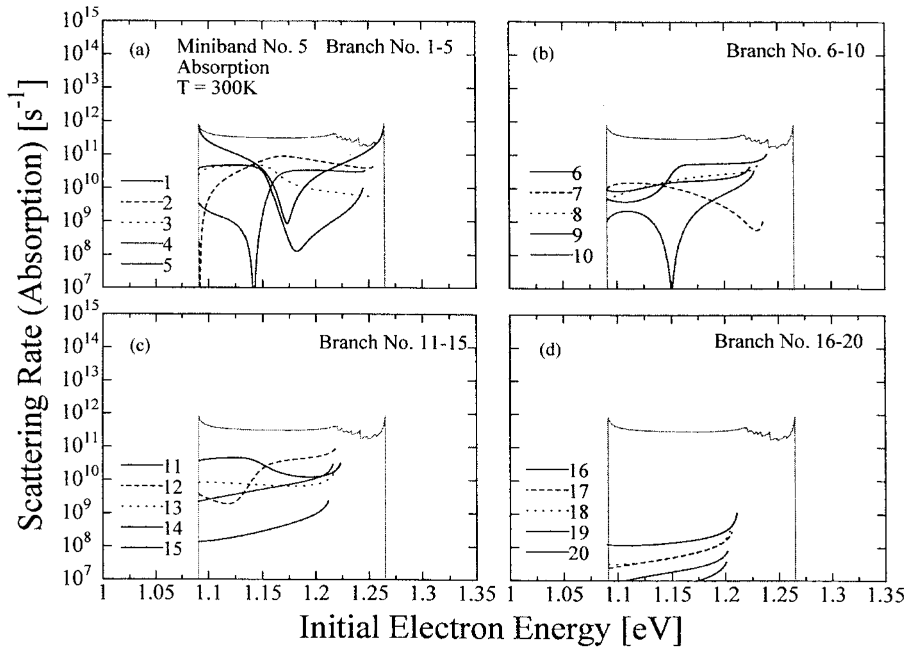

FIG. 7. Scattering rate for absorption process calculated for miniband 5 mediated by the phonons on branches (a) 1–5, (b) 6–10, (c) 10–15, and (d) 16–20. Gray curve shows total scattering rate for absorption, which is given by the sum of the results for each phonon branch.

The total scattering rate for absorption W, denoted by the gray curve, is given as the sum of the curves obtained for each phonon branch W_{b_p}. It is observed that the scattering rate mediated by the first, second, sixth, eleventh, and twelfth phonon branches are of the order of 10^{11}, and greatly contribute to W. On the other hand, the scatterings mediated by the fifteenth to twentieth phonon branches are so small that they have minimal impact on W. This is due to the small number of phonons in high-energy phonon branches. It is important to note that, when the initial electron energy is near the top of the miniband, high-energy phonon branches do not contribute to W. In this case, scattering events mediated by high-energy phonon branches are not allowed because the final electron states fall in the minibandgap lying above the fifth miniband. Therefore, the number of available phonon branches decreases with increasing initial electron energy, and ultimately, the lowest phonon branch is the only available one. This is the reason for the rapid decrease of phonon absorption at near the top of minibands. A similar effect occurs in emission processes shown in Figs. 8(a)–8(d), which causes reduction of phonon emission at near the bottom of the miniband. Of course, these phenomena and explanations are applicable to other minibands as well.

D. Energy relaxation rate

Figure 9 shows the energy relaxation rate as a function of initial electron energy. The calculation was performed at $T=300$ K, and the broken and solid lines show results for absorption and emission processes, respectively. The gray solid line is the total energy relaxation rate, which is defined as the sum of the results for absorption and emission. The energy relaxation rates are about 0.5×10^{11} s^{-1}, and the emission processes have larger values than absorption processes for the same reason as the scattering rates. As a result, total energy relaxation rate is positive at most energies. However, it has negative value at near the bottom of the minibands. This can be observed more clearly in Fig. 10, where

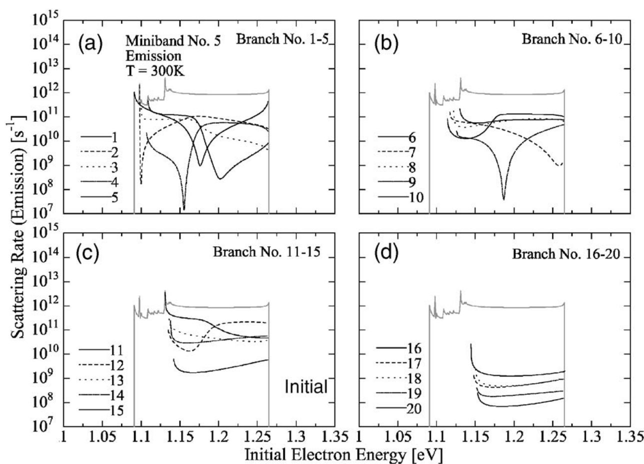

FIG. 8. Same plot as Fig. 7 calculated for emission process.

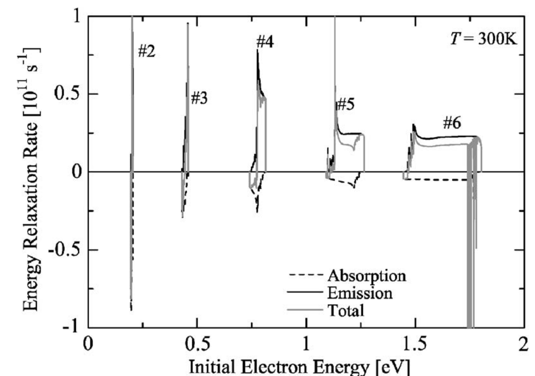

FIG. 9. Energy relaxation rate as a function of initial electron energy. Solid lines: emission processes; broken lines: absorption processes; and gray lines: total energy relaxation rate. The calculation was performed at $T=300$ K.

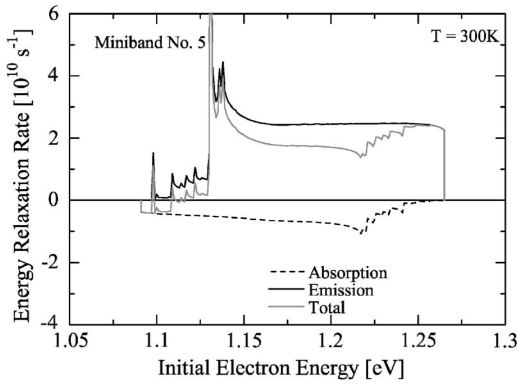

FIG. 10. Blow-up of the results for the fifth miniband shown in Fig. 9.

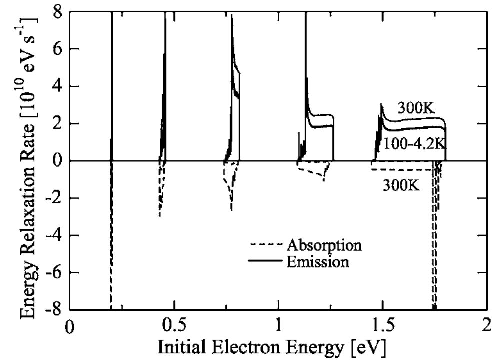

FIG. 12. Energy relaxation rate for absorption (broken line) and emission process (solid line) calculated for T=300, 100, 77, 33, 10, and 4.2 K.

the results calculated for electrons in the fifth miniband is shown. The negative energy relaxation rate is unique to the 1DSiQDA, and is not usually observed in the bulk Si or the SiQW. This occurs partly because the scattering rate for absorption process is larger than that for emission process, as seen in the inset in Fig. 6. Another reason is that the phonon emission at near the bottom of minibands are mediated only by low-energy phonons, and hence the energy relaxation rate for emission process is decreased.

E. Temperature dependence

Figure 11 shows temeperature dependence of the scattering rates for (a) absorption and (b) emission processes. The scattering rate for absorption decreases rapidly with decreasing temperature; $10^8 \sim 10^{10}$ at 77 K and $10^3 \sim 10^9$ at 4.2 K.

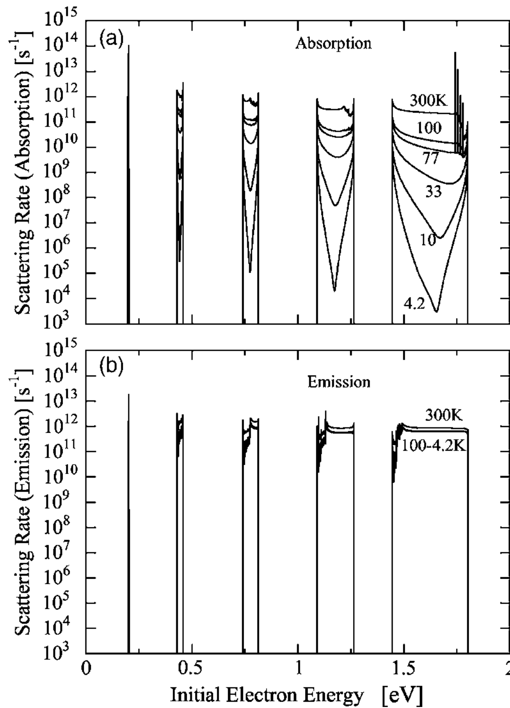

FIG. 11. Scattering rate for (a) absorption and (b) emission processes calculated for T=300, 100, 77, 33, 10, and 4.2 K.

This temperature dependence occurs solely from that of $n_{\mathbf{q}}$, and is described by the Bose-Einstein statistics. Note that the scattering rate becomes V-shaped as temperature decreases. This shape results from that of the scattering rate mediated by the lowest phonon branch, as seen in Fig. 7(a). This scattering becomes dominant at low temperature because majority of phonons exist at the lowest phonon branch. On the other hand, the scattering rate for emission process does not decrease once the temperature becomes lower than 100 K. Once $n_{\mathbf{q}}$ becomes much smaller than unity, $n_{-\mathbf{q}}+1$ term in Eq. (9) is approximated as unity. As a result, the scattering rate becomes independent of temperature.

Figure 12 shows temperature dependence of the energy relaxation rate calculated for absorption (broken line) and emission (solid line) processes. Once the temperature becomes below 100 K, the energy relaxation rate for emission process dominates the absorption process, as seen in the scattering rates. Because of this, the negative energy relaxation rate observed in Fig. 10 is not observed at low temperature. The negative energy relaxation rate, however, should be more prominent at high temperatures.

F. Suppression of interminiband scattering

One of the most unique features of the 1DSiQDA is suppression of the interminiband scattering. As the transverse energy can change during the interminiband scatterings, minibands are now redefined as allowed total energy ranges, which is obtained by superposing the minibands in Fig. 3(a) with added transverse energies.

Figure 13 shows such energy minibands. Electrons can take total energies within the filled energy ranges denoted as "Total." This is obtained by superposing the minibands in Fig. 3(a) with added transverse energies at various excitations, as shown in Fig. 13 for different excitation. In the calculation of the transverse energies, electron effective mass in Si was used.

Figure 14(a) shows minibandgap energies as a function of minibandgap number n. The nth minibandgap is defined as energy gaps between nth and $n+1$st minibands. Note that minibandgaps 1, 3, 6, 9, and 12 are above the maximum phonon energy denoted by the broken line. Interminiband scatterings over such minibandgaps are not allowed because

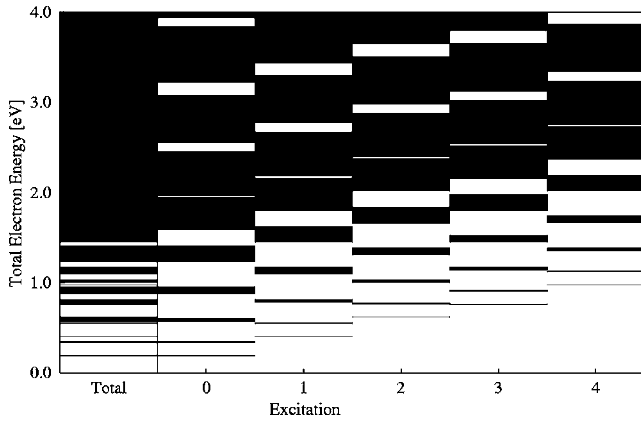

FIG. 13. Minibands considering transverse electron energy excitation. Excitation index indicates different transverse excitation energies, and "Total" denotes result obtained by superposing the minibands obtained for each excitation index.

of the energy conservation law. Considering that the number of phonons is extremely small at the maximum phonon energy, interminiband scattering rate over minibandgaps 2 and 13 would be virtually negligible. Figure 14(b) shows minibandgap energies calculated for $L_x=L_y=L_z=3.0$ nm and $L_x=L_y=L_z=7.0$ nm. When the dot size is 3.0 nm, most minibandgaps are larger than the phonon maximum energy, resulting in suppression of interminiband scattering over many minibandgaps. On the other hand, when the dot size is 7.0 nm, all minibandgaps are below the maximum phonon energy, and no interminiband suppression occurs.

IV. DISCUSSION

In this section, we discuss several issues regarding the theoretical assumptions and the simulation results.

Firstly, we discuss validity of the ideal 1DSiQDA structure. As mentioned in Sec. I, the ideal 1DSiQDA is a model to give theoretical footings for understanding the electron emission phenomena from PS and related structures,[12–15]

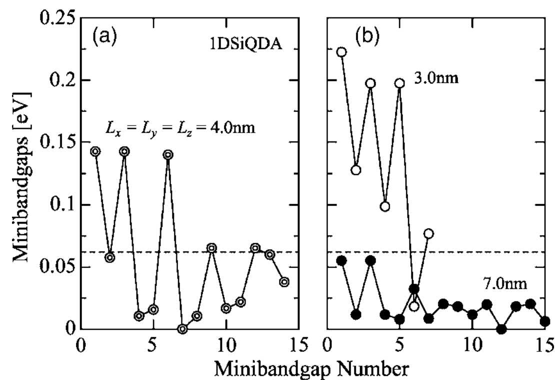

FIG. 14. Minibandgap energies as a function of minibandgap number n calculated for different Si dot sizes. (a) 4.0 nm, (b) 3.0 and 7.0 nm. The nth minibandgap is defined as energy gaps between nth and $n+1$st minibands. The broken lines indicate the maximum phonon energy in the 1DSiQDA, 0.062 eV.

poly-Si point contact transistors facilitating coherent quantum states of electrons,[18] electromechanical memory devices,[19] and so on. As for the PS devices,[12–15] several experiments indicate that the periodicity and one-dimensionality of the Si/oxide array are essential for efficient electron emission. In PS devices prepared under an appropriate anodization conditions, the sequential structure of silicon dot interconnected by thin oxide films has been observed in the samples formed on both single-crystal Si substrate[44] and poly-Si substrate[45] by transmission electron microscope (TEM) measurements. It has also been confirmed that the structures observed in these TEM photographs closely correlate to both the high emission efficiency and the ballistic feature of emitted electron energy distribution.[45,46] For the poly-Si point contact transistor and electromechanical memory devices, the Si dot size is well controlled and the structure is highly periodic.[18,19] Thus, our idealized model is a reasonable starting point to predict electronic/phononic properties at the best condition.

Secondly, we comment on the impact of the realistic phonon calculation introduced in Sec. II C. The major differences from the phononic states in mechanically homogeneous quantum wires are the phonon bandgaps [Fig. 4(a)], the distorted acoustic phonon waves [Fig. 5(a)], and the confined phonon waves [Fig. 5(b)]. The phonon bandgaps would not have significant influence on electron transport phenomena as far as electric field applied across the 1DSiQDA is small enough to exhibit minibands, in which allowed energy levels are continuous. The optical phonons confined in Si dots would not affect electron transport characteristics either, because the scatterings mediated by such high-energy phonon states are relatively weak, as shown in Figs. 7 and 8. However, the distorted acoustic phonon waves have certain influence on electron transport. It has been reported that the distorted acoustic phonon waves result in phonon-generated strain redistribution in the 1DSiQDA.[47,48] This effect eventually leads to reduction of the scattering potential of ADP scattering by about 20%. Therefore, the realistic phonon calculation is necessary in modeling the electron transport characteristics at energies where scattering mediated by low-energy phonon branches are dominant.

Finally, we discuss electron transport characteristics along the 1DSiQDA. As mentioned in Sec. III C, the intraminiband scattering rates are slightly higher than that calculated for bulk Si.[30] Furthermore, several lowest minibands, where the majority of electrons exists assuming a Maxwell-Boltzmann distribution, have small dispersion, leading to high miniband effective mass. Therefore, electron mobility along the 1DSiQDA becomes much smaller than that of the SiQW. This is quite obvious because the oxide layers impede electron transport along the x direction. However, negative energy relaxation rate shown in Sec. III E, and suppression of the interminiband scatterings mentioned in Sec. III F are unique to the 1DSiQDA. These characteristics might become important when nonequilibrium electron transport is considered. Hot electrons injected at energies within which the energy relaxation rate is negative might gain energy by absorption of phonons, maintaining the initial energy for long duration of time. In addition, as the interminiband scatterings are restricted in some of the minibands, electrons in mini-

bands above large minibandgaps keep the bottom energy of the miniband, as predicted by Sakaki for the polar-optical phonon scattering in GaAs/AlAs superlattice structures.[43] Thus, insertion of the oxide layers in a SiQW leads to low electron mobility, but instead, it might lead to longer energy relaxation time for hot electrons.

V. CONCLUSION

The electronic/phononic states and their interactions in the 1DSiQDA structure under low electric field condition have been theoretically investigated. The electronic states were obtained by solving the Schrödinger equation in the Kronig-Penny potential. The approximate expression for the phonon wave functions in the 1DSiQDA were developed, and the one-dimensional phonon wave and dispersion relation were numerically simulated using the linear atomic chain model. The simulated dispersion relation showed the acoustic phonon modes, the phonon bandgaps, and the confined optical phonon modes. It has been shown that the electron-phonon scattering rate can be reduced to the one-dimensional expression. Using the simplified expression, intraminiband scattering rates and energy relaxation rates have been simulated both for absorption and emission processes. The scattering rate varies from 10^{12} to 10^{14}, depending on the initial electron energy. The scattering rate for absorption/emission processes rapidly decreases at near the top/bottom of minibands due to the limited number of phonon branches which can mediate the scattering processes. The scatterings mediated by the first, second, sixth, eleventh, and twelfth phonon branches are of the order of 10^{11}. On the other hand, the scatterings mediated by the fifteenth to twentieth phonon branches are so weak that they have minimal impact on the total scattering rate. The negative energy relaxation rate has been observed near the bottom of minibands, which is due to larger scattering rate for absorption process and smaller phonon energy mediating the scatterings for emission process. The temperature dependences of the scattering rate and the energy relaxation rate were also investigated, and revealed that the scattering rate for absorption decreases rapidly with decreasing temperature. The energy relaxation rate for emission process dominates the absorption process, once the temperature drops down to 100 K. Because of this, the negative energy relaxation rate is not observed at low temperature.

ACKNOWLEDGMENTS

The authors would like to thank Dr. Armour of Nottingham University for his helpful discussions. The authors are also indebted to Dr. D. Williams of Hitachi Cambridge Laboratory and Prof. S. Oda of Tokyo Institute of Technology for their support.

*Electronic address: drsuno@phy.cam.ac.uk; also at CREST JST (Japan Science and Technology), Shibuya TK Bldg., 3-13-11 Shibuya, Shibuya-ku, Tokyo 150-0002, Japan.

†Also at CREST JST (Japan Science and Technology), Shibuya TK Bldg., 3-13-11 Shibuya, Shibuya-ku, Tokyo 150-0002, Japan.

[1] A. B. Fowler, A. Hartstein, and R. A. Webb, Phys. Rev. Lett. **48**, 196 (1982).

[2] R. A. Smith and H. Ahmed, J. Appl. Phys. **81**, 2699 (1996).

[3] J. H. F. Scott-Thomas, S. B. Field, M. A. Kastner, H. I. Smith, and D. A. Antoniadis, Phys. Rev. Lett. **62**, 583 (1989).

[4] Y. S. Tang, G. Jin, J. H. Davies, J. G. Williamson, and C. D. W. Wilkinson, Phys. Rev. B **45**, 13799 (1992)

[5] Y. Takahashi, A. Fujiwara, and K. Murase, Semicond. Sci. Technol. **13**, 1047 (1998)

[6] H. Namatsu, K. Kurihara, M. Nagase, and T. Makino, Appl. Phys. Lett. **70**, 619 (1996)

[7] A. T. Tilke, F. C. Simmel, H. Lorenz, R. H. Blick, and J. P. Kotthaus, Phys. Rev. B **68**, 075311 (2003).

[8] W. J. Skocpol, P. M. Mankiewich, R. E. Howard, L. D. Jackel, D. M. Tennant, and A. D. Stone, Phys. Rev. Lett. **56**, 2865 (1986)

[9] A. G. Cullis, L. T. Camham, and P. D. J. Calcott, J. Appl. Phys. **82**, 909 (1997).

[10] R. L. Smith and S. D. Colins, J. Appl. Phys. **71**, R1 (1992)

[11] L. T. Canham, Phys. Status Solidi B **190**, 9 (1995).

[12] N. Koshida, T. Ozaki, X. Sheng, and H. Koyama, Jpn. J. Appl. Phys., Part 1 **34**, L705 (1995).

[13] N. Koshida, X. Sheng, and T. Komoda, Appl. Surf. Sci. **146**, 371 (1999).

[14] T. Komoda, X. Sheng, and N. Koshida, J. Vac. Sci. Technol. B **17**, 1076 (1999).

[15] K. Nishiguchi, X. Zhao, and S. Oda, J. Appl. Phys. **92**, 2748 (2002).

[16] S. Uno, K. Nakazato, S. Yamaguchi, A. Kojima, N. Koshida, and H. Mizuta, IEEE Trans. Nanotechnol. **2** 301 (2003).

[17] G. d. Sanders and C. J. Staton, Phys. Rev. B **48**, 11067 (1993).

[18] M. Khalafalla, Z. Durrani, and H. Mizuta, Appl. Phys. Lett. **85**, 2262 (2004).

[19] Y. Tsuchiya, K. Takai, N. Momo, S. Oda, S. Yamaguchi, T. Shimada, and H. Mizuta, *27th International Conference on Physics of Semiconductors* (ICPS-27), Arizona, July 2004, M3-004.

[20] H. Noguchi, J. P. Leburton, and H. Sakaki, Phys. Rev. B **47**, 15593 (1993).

[21] J. E. Stocker, J. P. Leburton, H. Noguchi, and H. Sakaki, J. Appl. Phys. **76**, 4231 (1994).

[22] S. Adachi, J. Appl. Phys. **58**, R1 (1985).

[23] B. Bhushan and X. Li, J. Mater. Res. **12**, 54 (1992).

[24] M. T. Kim, Thin Solid Films **283**, 12 (1996).

[25] S. Takagi, J. Koga, and A. Toriumi, Jpn. J. Appl. Phys., Part 1 **37**, 1289 (1998).

[26] R. W. Morse, J. Acoust. Soc. Am., **22**, 219 (1950).

[27] G. Fishman, Phys. Rev. B **36**, 7448 (1987).

[28] T. Yamada and J. Sone, Phys. Rev. B **40**, 6265 (1989).

[29] O. Madelung, *Introduction to Solid-state theory* (Springer, New York, 1996).

[30] C. Jacoboni and L. Reggiani, Rev. Mod. Phys. **55**, 645 (1983).

[31] H. Tanino, A. Kuprin, H. Deai, and N. Koshida, Phys. Rev. B **53**, 1937 (1996).

[32] S. M. Sze, *Physics of Semiconductor Devices* (Wiley, New York,

1981).
[33] V. K. Arora and F. G. Awad, Phys. Rev. B **23**, 5570 (1981).
[34] W. A. Harrison, *Solid State Theory* (McGraw-Hill, New York, 1970).
[35] S. Zoilner, S. Gopajan, and M. Cardona, J. Appl. Phys. **68** 1682 (1990).
[36] M. Lundstrom, *Fundamentals of Carrier Transport* (Cambridge University Press, Cambridge, 2000).
[37] A. Kojima and N. Koshida, Phys. Status Solidi A **197**, 452 (2003)
[38] M. V. Fischetti, Phys. Rev. Lett. **53**, 1755 (1984).
[39] M. V. Fischetti, Solid-State Electron. **31**, 629 (1988).
[40] O. Koblinger, J. Mebert, E. Dittrich, S. Döttinger, and W. Eisenmenger, Phys. Rev. B **35**, 9372 (1987).
[41] H. Mizuta and T. Tanoue, *The Physics and Applications of Resonant Tunneling Diodes* (Cambridge University Press, Cambridge, 1995).
[42] N. W. Ashcroft and N. D. Mermin, *Solid State Physics* (Saunders College Press, Saunders, 1976).
[43] H. Sakaki, Jpn. J. Appl. Phys., Part 2 **28**, L314 (1989).
[44] N. Koshida and N. Matsumoto, Mater. Sci. Eng., R. **40**, 169 (2002).
[45] T. Ichihara, T. Baba, T. Komoda, and N. Koshida, J. Vac. Sci. Technol. B **24**, 1372 (2004).
[46] T. Ichihara, T. Hatai, K. Aizawa, T. Komoda, A. Kojima, and N. Koshida, J. Vac. Sci. Technol. B **22**, 57 (2004).
[47] S. Uno, N. Mori, K. Nakazato, N. Koshida, and H. Mizuta, *Extended Abstract of International Conference on Solid State Devices and Materials*, Tokyo, September 2004, H-1-5.
[48] S. Uno, N. Mori, K. Nakazato, N. Koshida, and H. Mizuta J. Appl. Phys. **97**, 113506 (2005).